Appendix I

Improved Seismic Locations and Location Techniques

By:

SM Spottiswoode and LM Linzer

Research Agency: CSIR: Division of Mining Technology
Project Number: SIM020304
Date: December 2004

Table of contents

List of figures

List of tables

1 Introduction

1.1 Original motivation, from the project proposal

Current seismic event location algorithms are based on time residuals and velocity models. Event locations based on these typically have errors of the order of 30 to 100 metres, depending on the distribution of the seismic sensors, their distance apart from each other, and factors such as the mining geometry and the geotechnical environment. Seismic location accuracy has not materially improved over the last ten years.

The most effective way to improve location accuracy is to install more geophones or accelerometers, but this comes at a price. It means also, that the seismic system becomes more sensitive, becoming able to record many more events, which places more pressure on seismic staff. This extra data is either ignored, or extra staff must be obtained to do all the processing. If some of the data are ignored, there is no guarantee that the data selected for processing are the best recorded by the system. Quality control becomes more difficult, because there are more data to deal with. The overall quality of the data is likely to decline in this scenario because of the increase in the sensitivity of the system, hence the number of small events recorded, and a poorer signal: noise ratio for the smaller events. There is thus no guarantee that all the extra data will be beneficial at all, despite the extra costs incurred through recording and processing. One benefit is gained: the larger events will be recorded by more stations, which should, on average, result in better source parameter determinations.

The cost: benefit of increasing system sensitivity is thus probably negative; there is no indication from industry that mines with sensitive systems have derived any more benefits than mines with less sensitive systems. This is particularly true for prediction, which remains just as elusive regardless of the sensitivity of the system. It therefore appears that there is a practical sensitivity threshold below which it is senseless to venture. Most mines derive substantial benefits from seismic management when employing data with local magnitude down to zero. Increasing sensitivity of such a system to local magnitude –1.0 will probably bring in about 10 times as many events, but it will almost certainly not produce a clearer picture of seismicity on the mine. Examples of this can be found with sensitive networks in the Carbon Leader Reef Shaft Pillars at Western Deep Levels, where it has been noted that the potential to predict damaging seismicity has not been enhanced by increased sensitivity.

Thus, the quest for more data in order to improve the seismic service is probably incorrect. It would be far more beneficial to improve the quality of the data already being recorded and processed without adding any sensors to the existing systems. The most important seismic parameter is its location, because the value of all other seismic parameters, starting with moment and energy, are dependent upon the location. As far as is known, there is little or no work done on the error of seismic source parameter determinations. This project aims to improve seismic locations by an order of magnitude, that is, to reduce the error of location by an order of magnitude, without requiring any changes or additions to existing mine-wide seismic systems. The waveform similarity technique of seismic location has already demonstrated its ability to achieve this goal, however, there are limitations to its use, and these should be investigated and removed wherever possible. Other location improvement techniques should be evaluated for their potential along with the waveform similarity technique. This project also intends to address the errors with which seismic source parameters are determined; it appears that this can only be objectively achieved with a combination of laboratory studies and field tests.

The second real problem with seismic monitoring is the continued manual location methods employed to obtain seismic locations. Automatic location algorithms exist, but they still fail. The

reasons they do are either unknown or unreported. New neural network-based algorithms have demonstrated startlingly good ability to identify seismic traces in noisy data. These can probably be used firstly to “remove” noise from the seismograms, and secondly to determine the P- and S-wave onsets accurately by automatic means from a better quality seismogram. In order to do this, noise sources and their effects on the seismograms should be investigated; the effect of noise on accurate seismic parameter determination should also be quantified.

All the above-mentioned work should be confined to seismic events with local magnitudes of 0.0 and larger, and aimed at typical mine-wide seismic systems with 10 to 30 sensors covering an area about 5 km across. If the results achieve the stated goals of an order of magnitude reduction in location error and a reliable automatic location algorithm, then the door to real-time seismic monitoring and analysis will have been opened.

2 Investigate various location techniques

2.1 Literature review of waveform similarity techniques

One of the oldest problems in seismology, which is still the subject of active research, is the determination of the hypocentre or focus of the source. The location of an event is the most important seismic parameter because all other parameters (e.g. moment, energy, etc.) are dependent on it. Additionally, the interpretation of seismogenic features is critically dependent on the accuracy of the estimated hypocentres. Hypocentral scattering also affects other applications that involve parametric data, for example, spatio-temporal seismicity trends.

Uncertainties in event locations can be grouped into two categories: random errors and systematic errors. Random errors are generally caused by errors in the arrival times of picked wave phases. Such errors include picking inconsistencies, the misidentification of seismic phases, variations in signal-to-noise ratios, and human subjectivity. Systematic errors are caused by the variation in the rock mass structure between the seismic source and the receiver. Such variations could be due to the local geology, the presence of stopes and associated fractured rock and result in ray path focusing and defocusing of the elastic wave between source and receiver.

There are a number of methods described in the literature to reduce hypocentral scattering, most of which are based on time residuals and a velocity model. Earthquake relocation techniques have recently been markedly improved by using a number of different techniques, all of which are highlighted in the following survey, and covered in broader detail in the main report. Jones & Stewart (1997) presented a statistical approach to reducing hypocentral 'fuzziness' caused by pick inconsistencies. This method is also referred to as 'collapsing' and is based on the assumption that the pick errors form a Gaussian distribution. According to Rowe et al. (2002) synthetic tests as well as comparisons to results from manual repicking of recorded data sets have demonstrated considerable success. These researchers suggest that collapsing, in combination with techniques for adjusting the velocity model and/or near-surface static corrections, may be a good approach to improve delineation of seismogenic features. The advantage of collapsing is that waveform data is not required. However, the collapsing technique can be prone to artefacts.

Fehler et al. (2000) propose a method known as 'JHD-collapsing'. This method is based on the same basic assumption of Jones & Stewart (1997): that there is a greater clustering on actual earthquake locations than there is in locations determined using conventional techniques. The difference is that the method is implemented as part of the Joint Hypocentre Determination (JHD) process so it operates on raw travel-time data rather than on derived hypocentres. These researchers found that the JHD-collapsing method resulted in the hypocentres being significantly more clustered than those found using JHD alone.

The effects of errors in the knowledge of the earth structure can be minimised by using relative location methods (e.g. Got et al., 1994). These methods apply if the hypocentral separation between two earthquakes is small compared to the event-station distance and the scale length of the velocity heterogeneity. Under these conditions, the ray-paths between the source region and receiver can be considered common, and the difference in travel times for two events observed at one station can be attributed to the spatial offset between the events with high accuracy.

The accuracy of the relative locations can be further enhanced if the events are clustered spatially and have similar waveforms. The waveform similarity is exploited to pick precise arrival times (e.g. Got et al. 1994; Nadeau et al., 1995; Spottiswoode & Milev, 1998; Rubin et

al., 1999). The maps of the enhanced locations determined using these techniques show details not evident from locations computed using conventional methods.

Waldhauser & Ellsworth (2000) have developed a 'double-difference' location algorithm to sharpen the seismogenic source volume image of large numbers of earthquakes. The location method incorporates absolute travel-time measures (obtained from catalogue data) and/or cross-correlations P- and S-wave differential travel-times (derived from cross-spectral methods). The residuals between the observed and theoretical travel-time differences are known as 'double-differences' and are minimised for pairs of earthquakes at each station while linking together all observed event-station pairs. These researchers applied the double-differences algorithm to relocate earthquakes on the northern Hayward fault. Figure 2.1.1 (a) shows the locations of the events recorded by the NCSN (Northern California Seismic Network) recorded between 1984 and 1998. Figure 2.1.1 (b) shows the double-difference locations obtained solely from catalogue travel-time differences. It is evident that the relocation method collapses the epicentres into a narrow zone of seismic activity. The relocated events derived with the combined set of catalogue and cross-correlation data are shown in Figure 2.1.1(c). The double-difference locations shown in Figure 2.1.1(c) reveal a focussed picture of seismicity, with most of the events aligning in depth along linear, horizontal streaks (Waldhauser et al., 1999).

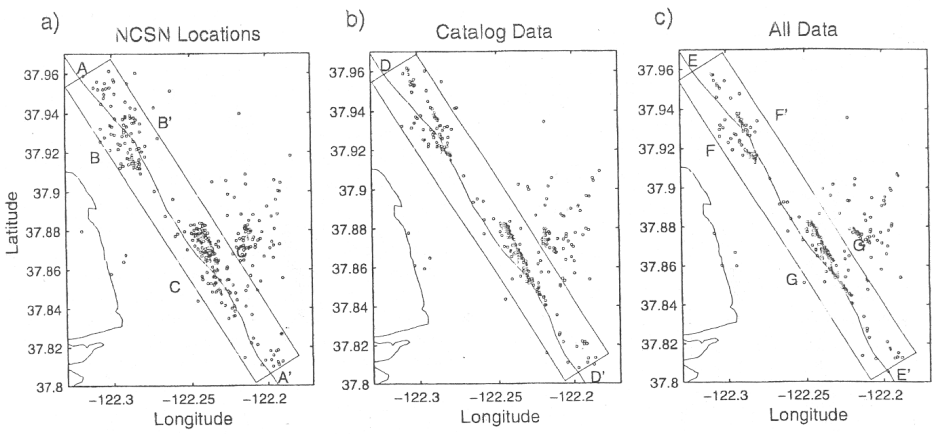

Figure 2.1.1 (a) NCSN locations (b) double-difference locations obtained using catalogue data (c) relocated events derived using a combined set of catalogue and cross-correlation data (from Waldhauser & Ellsworth, 2000).

Sambridge & Kennett (2001) applied a recently developed direct search method for inversion known as the neighbourhood algorithm (NA) to the location problem. The algorithm uses randomised sampling of a 4-dimensional hypocentral parameter space, to search for solutions with an acceptable fit to data. At each stage, the hypocentral parameter space is partitioned into a series of convex polygons called Voronoi cells. Each cell surrounds a previously generated hypocentre for which the fit to the data has been calculated. New hypocentres are generated randomly in the neighbourhood of those hypocentres with smaller data misfit as the algorithm proceeds. In this way, all previous hypocentres guide the search and the more promising regions of parameter space are preferentially sampled.

The waveform similarity method is becoming increasingly popular in earthquake studies. For example, the most recent issue of the Bulletin of the Seismological Society of America (Issue: 2002 - volume 92 - issue 5) has two papers (out of 33 papers) on the topic, namely Rubin (2002) and Got et al. (2002).

A common thread to all the papers to date on the topic is that multiplets with almost identical waveforms are fairly common, but not the rule. The degree of similarity decreases with inter-event distance, but in a controlled manner that can be used with advantage. When processing for large mine data sets, each event of large data sets will be compared with all nearby events.

2.2 Type "A" events - "fracture-dominated" rupture of competent rock or development blasts.

2.2.1 Abstract

The paper by Richardson and Jordan (2002) proposed that many of the smaller events were caused by a newly identified "fracture-dominated" mechanism (Type A) and that the large "friction-dominated" (Type B) events had some mechanism-associated value of M_{MIN}. In this note, we show that the Type A events are development blasts and that M_{MIN} can be explained by the triggering logic of the seismic systems. Type A events are development blasts and can therefore be used for improving velocities and locations.

2.2.2 Introduction

During 2001, Prof Tom Jordan and his student Eliza Richardson were working on interpretation of mine seismic events in terms of clusters of small seismic events, which they called "Type A", which they interpreted as "fracture dominated" events whereas the larger, "Type B", events were interpreted as "friction-dominated" events. Both workers were expected to be at the ISSI seminar in March 2002. As some of us did not agree with the interpretation of the "Type A" events, we presented a brief talk putting our case that the Type A events were actually all or almost all development blasts and therefore could not simply be interpreted as providing insights into fundamental rock mass behaviour (Finnie et al, 2002). As expected, there was lively discussion on this topic. Many of the audience supported our interpretation. Others, including senior ISSI personnel, supported the Richardson-Jordan model[1]. They went further and claimed that blasts were too small to trigger their systems. The amount of true discussion was limited.

In the meantime, a paper had been submitted and was later published in the Bulletin of the Seismological Society of America (BSSA) on the topic (Richardson and Jordan, 2002). As the BSSA is not widely read within the South African mining industry and the impact of their conclusions in South Africa was marginal, our horizons became clouded by budget restraints and pressure of work. As a result, we did not feel that a response was "cost-effective" at the time and allowed the matter to rest.

The DAFSAM meeting between 23rd and 27th September 2002 in Parys, South Africa provided a good opportunity to respond to the Richardson and Jordan (2002) paper. Prof Jordan was attending and was expected to talk again about this theory. One of us (Spottiswoode) prepared a talk for this meeting. This section is based on that talk.

There were detailed discussions both with Prof Jordan and with other attendees during and after the talk. As the attendees at this meeting were all well respected scientists, the discussions were open. At the end, none of the participants, including Prof Jordan, disputed the evidence or conclusion that Type A are all or almost all blast events.

Why is this presented in a SIMRAC project report on improved location methods? The reason is simply that, if the Type "A" events can be shown to be blasts and not induced events, then the location of these events can be used to calibrate velocity models for improving event locations.

2.2.3 Spatio-temporal distribution of Type "A" events.

We follow the Richardson and Jordan (2002) identification method by using space-time clustering to identify sequences of Type "A" events. Groups of events within 100 m and 45 minutes of one another and with M(Mo) < 0.5 were identified in a data set from a mine. In

1 The pressure on the first author of our talk was too great and he declined to speak. The second author spoke in his place.

Figure 2.2.1 and Figure 2.2.2, we show 10 such clusters together with all M>2 events within the same time periods.

Richardson and Jordan (2002) acknowledged that the clustered events were in some way connected with blasting, suggesting that they were some sort of aftershock. This might be expected if the development took place in highly stressed ground, but not in the low field stress of follow-behind haulages. Finally, they used inter-event distances of 100m as part of their identification of "Type A" events.

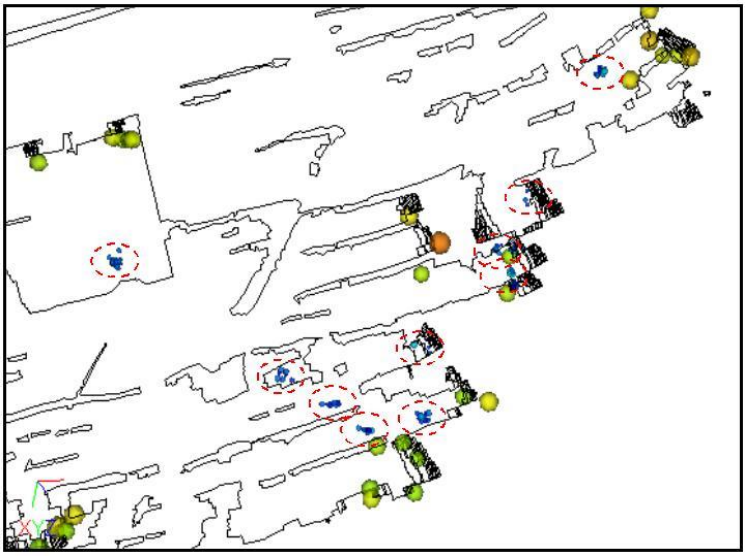

Figure 2.2.1: Clusters of Type "A" events as small blue circles within dashed red ellipses and all M>2 events as larger green yellow or red circles. Some of the clusters consisted of events from different days. Mine outlines at a number of mining steps are shown. It can be seen that the larger events plot, as expected, on active faces or nearby stationary abutments or pillars. The smaller events were in areas of known or expected development blasting.

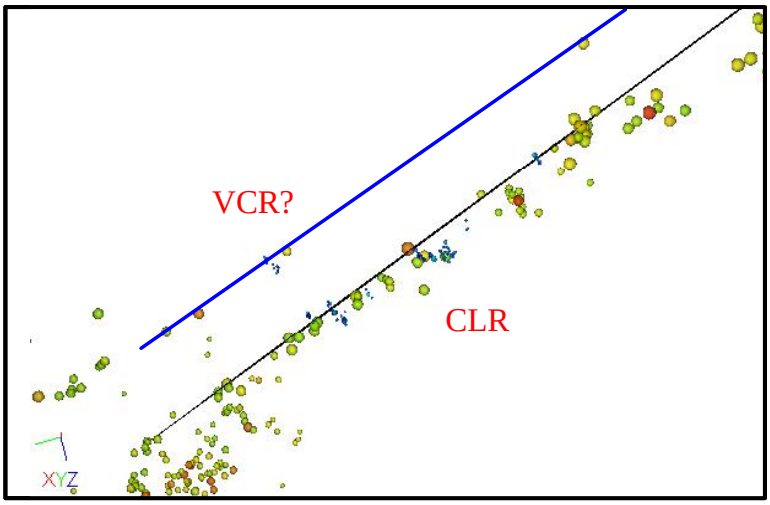

Figure 2.2.2: Cross-section through Figure 1.3.3.1. The middling between the Carbon Leader Reef (CLR) and the Ventersdorp Contact Reef (VCR) is about 600 m indicating that the spread of locations normal to reef exceeds 100 m. This spread increases towards the down-dip edge suggesting a need for improving the velocity model for locations.

Each of the clusters occurred during the blasting times. The time distribution of a number of sequences is plotted in Figure 2.2.3 and shows a constant rate of events, with no evidence of gradually decreased seismicity rate that would appear as an exponential plot.

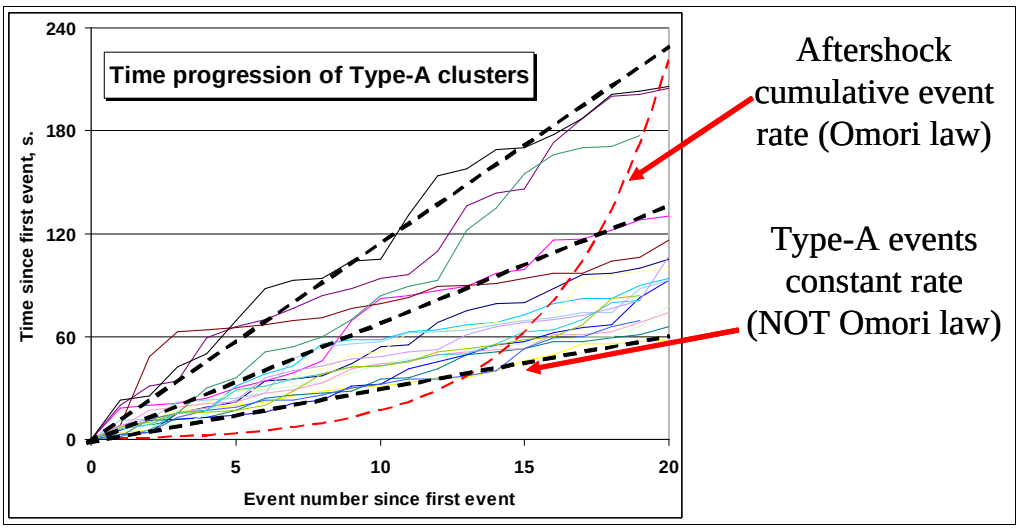

Figure 2.2.3: Time distribution of 20 clusters of events. The X and Y coordinates are switched from the normal sense for ease of plotting the data. An exponential line representing a typical Omori-type aftershock distribution is shown. The event rate, however, appears to be constant as shown by the three straight dashed lines shown for comparison.

Discussions with suppliers of explosives to mines in the Carletonville area elicited the following points:

1. Development blasting still takes place on the Carletonville mines using slow-burning igniter cord between charges.
2. 1000s of such charges are set off per month on a typical mine
3. Mines have been moving to electronic stope blasting
4. A development blast sequence lasts for several minutes.

All these points are compatible with Figure 2.2.3.

Can Type "B" only occur above some $M_{MIN} \approx 0.5$?

The main argument put forward by Richardson and Jordan (2002) for Types A and B events being different populations was based on the frequency-magnitude distributions (Figure 2.2.4). Their argument was that the smaller events formed the population of events below the M_{MIN} marked in Figure 2.2.4. The other events showed a distinct decrease in the number of events less than M_{MIN}. They argued that this M_{MIN} was **not** a function of the network sensitivity because the smaller Type A events were consistently recorded.

Figure 2.2.5 shows that Types "A" and "B" events may also be obtained separately from spatially separated data sets.

We reject this argument using the following two facts:

1. Type A events are more energetic for the same seismic moment than Type B events.
2. The ISSI networks used a system of triggering based on peak velocity.

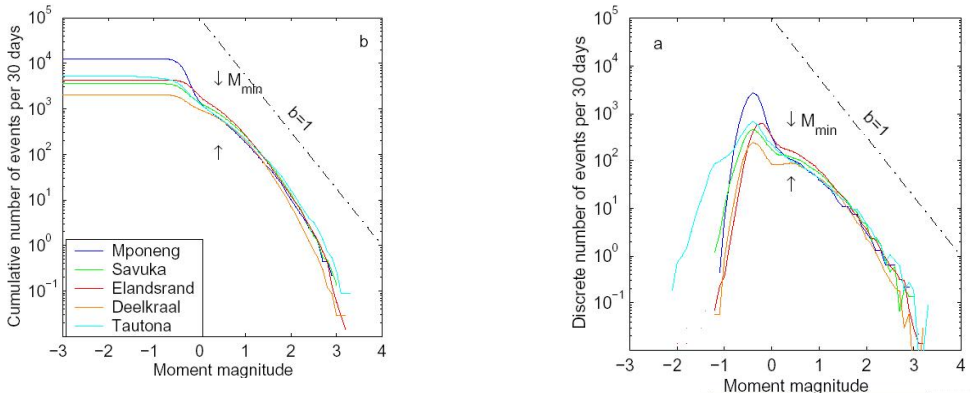

Figure 2.2.4: Discrete (a) and cumulative (b) Gutenberg-Richter (Frequency-magnitude) distributions from Figure 3 of Richardson and Jordan.

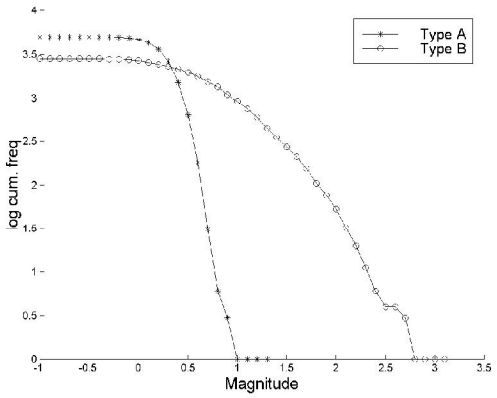

Figure 2.2.5: Cumulative Gutenberg-Richter distributions from Finnie et al (2002). The data set for Type A events was obtained from an area that was being developed but in which there was no active stoping. The data for Type B events were obtained from an area of mature stoping and no development blasting.

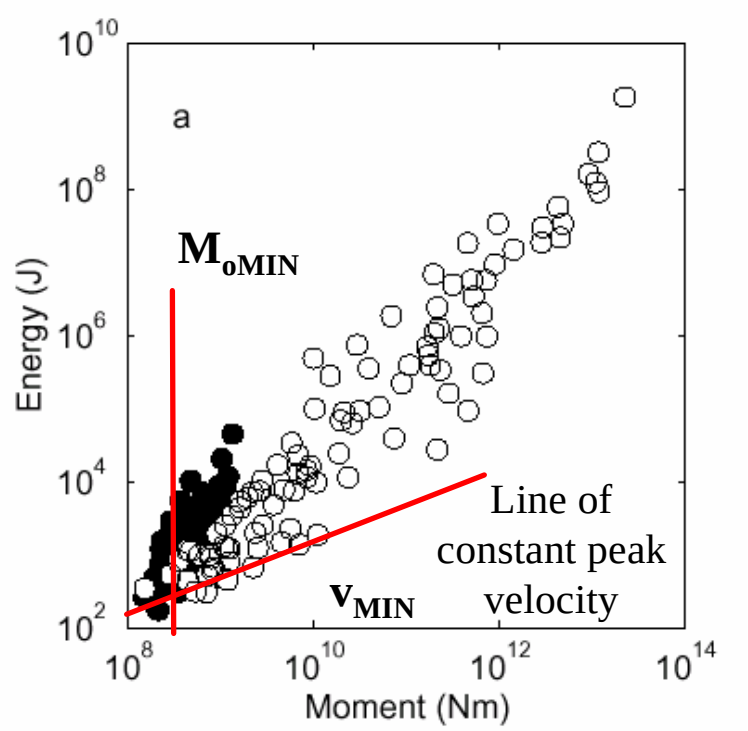

Figure 2.2.6: The graph and symbols are from Figure 9 of Richardson and Jordan (2002). We have added two construction lines, a line showing a suggested M_{MIN} for Type B and a line of constant v_{MIN} as a proposed trigger threshold.

The suggested network threshold marked in Figure 2.2.6 is based on the following analysis based on standard seismic source scaling laws (see also Figure 2.2.7):

$E \sim v^2 \times T$

$Mo \sim v \times T^2$

Therefore: $E^2/Mo \sim v^3$

Where E = seismic energy,

Mo = Seismic Moment,

v = peak velocity and

T = Dominant period.

The construction line in Figure 2.2.6 has a slope of +2 on the log-log scale representing, as stated, a line of constant velocity.

We conclude therefore that the trigger threshold ("smallest value") for both Type A and Type B events is set by their peak velocity, not by their moment value and that the higher M_{MIN} for Type-B events results directly from the lower apparent stress of Type-B events.

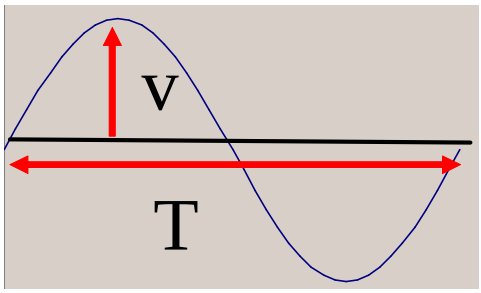

Figure 2.2.7: A sine wave as an elemental description of a seismic source pulse in the far field.

Again we ask: "Can Type "B" only occur above some $M_{MIN} \approx 0.5$?" Richardson and Jordan contended that the evidence pointed to an answer of "yes". We contend that the facts of the triggering have resulted in an apparent separation of the two populations.

It remains for us to address the fact that Type A events have higher E/Mo ~ apparent stress values than the Type B events. Our argument will be completed by consideration of a 140 Kg blast recorded and analysed by Milev et al (2001). They found (Figure 2.2.8) that this blast was recorded with about three times the apparent stress of induced events that located in the same area.

The estimated seismic moment of the 140 Kg blast was $4.5*10^{10}$ N-m. A single charge of a single development blast is 1 Kg. Assuming simple scaling, the equivalent seismic moment for such a blast is $4.5*10^{10} / 180 = 2.5 * 10^{8}$ N-m, equivalent to a Moment-Magnitude, M(Mo) = -0.4. This corresponds well to a typical Type "A" event.

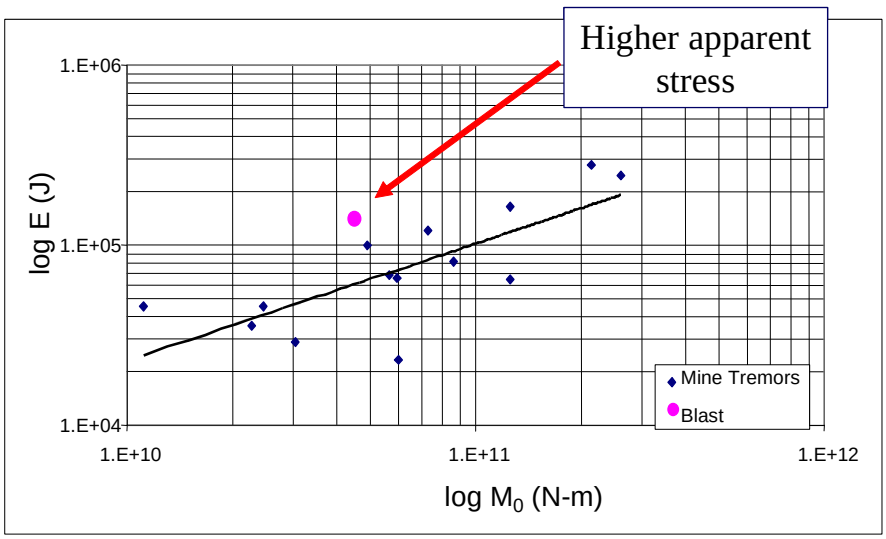

Figure 2.2.8: Graph of radiated energy as a function of Seismic Moment for a blast event and mining-induced events in the same area.

2.3 Conclusions

Type-A events are development blasts

1. Mines still use slow-burn fuses, particularly at development ends
2. A 1kg (development) charge generates $M \approx -0.4$.
3. The type "A" event rate is approximately constant and NOT Omori-like

The suggestion by Richardson and Jordan (2002) that there is a characteristic value of M_{MIN} for Type-B events that is above the typical M of type A events is a function of the type of network triggering. Type A events are development blasts and can be used for calibrating seismic velocities of mine networks.

2.3.1 Acknowledgements in connection with the DAFSAM talk in 2002.

Eliza Richardson kindly provided a preprint of the Richardson-Jordan paper prior to publication. I would like to thank George Craft, Hannes Redelinghuys and Hennie Enslin at African Explosives Limited (AEL) for discussions on development blasting. AEL are the main suppliers of explosives to the Carletonville area mines.

2.4 Location improvement techniques

2.4.1 Introduction.

Spottiswoode and Milev (1998) and Cichowicz (Method 2) (2003) provided a description of the classical relative location method. Arrival times are adjusted by corrections for each arrival time based time residuals from a chosen "master" event. These adjusted arrival times are then used to locate events close to the master event.

Following Cichowicz (2003, equation (8)), the time residual e_{ij} for any event *i* at station *j* and phase *c* (P or S) can be defined as:

$$e_{ij} = T_{ij} - t_{oi} - d_{ij} / V_{ci} \qquad 2.4.1$$

where t_{oi} = origin time of event *i*

T_{ij} = Picked arrival time of event *i* at site *j*.

d_{ij} = Hypocentral distance from event *i* to site *j* and

V_{ci} = Assumed phase velocity (P or S) along the ray path.

In this study, we obtain the "best" least squares absolute location by minimising $\sum e_{ij}^2$ or relative location by minimising $\sum (e_{ij} - e_{kj})^2$, where event *k* is the master event used to locate event *i*. The essential background to the relative location method is the recognition that the largest error in a single-event location comes from uncertainties in the phase velocity V_{ci}. The time residual e_{ij} is similar in value for events occurring much closer to one another than to any particular geophone site. For example, if the ray-paths travel through rock that is anomalously fast, then e_{ij} will be positive. For two identical events recorded by the same geophones with the same arrivals, the time residuals will be identical.

The conventional relative location method with master event requires an identified event, or master event, that is to be used to improve the relative location accuracies of all nearby events. This certainly has the potential to reduce scatter and improve the grouping of events that occur in a cluster. This improved grouping improves the "sharpness" of the locations, but suffers from several disadvantages:

1. The selection of the master event is subjective.
2. Data from sites that did not record the master event are lost for the other events.
3. The benefit of using the master event decreases with distance from it.
4. The absolute locations are only improved to about the same degree as the absolute location of the master event itself.

2.4.2 Hybrid absolute-relative location method.

During the course of the project, we developed a hybrid absolute-relative location method. The hybrid approach followed was similar to that used by Andersen (now Linzer) and Spottiswoode (2001) for moment tensor inversions. In developing the hybrid method, we have attempted to overcome the disadvantages of the master event method listed above:

1. All events may act as master events
2. All sites that record events are used.
3. Events are influenced by, and influence, nearby events.
4. Events with known locations will keep a control on the absolute locations of all events.
5. Development blasts are such events.

Although development blasts are small and are recorded at a limited number of geophone sites, their locations are well constrained. If we knew their full (X, Y, Z & T) location, even a single arrival at a single site would provide some useful information. This would require placing a geophone at the blast itself. Under normal conditions where this does not happen, we can start using them for improving locations as soon as the blasts are associated with development of a particular tunnel. The face position at the time of the blasts is desirable, but even the knowledge that the blast took place on a line can be used.

An algorithm (MLOC) is currently being developed to perform hybrid absolute-relative locations. The central theme of this method is that each event is located by minimising the square of a weighted average of absolute (uncorrected) and relative (corrected) time residuals:

$$\sum (e_{ij} - w_{rel} \times e_{kj})^2 \qquad 2.4.2$$

where w_{rel} is increased from 0.0 to 1.0.

This algorithm operates as follows:

1. Store event arrival times and locations of a set of events.
2. Start by applying a weight of $w_{rel} = 0.0$, in the normal fashion, as if an absolute location was being determined.
3. Calculate time residuals e_{ij} of each event *i* at station *j* and phase *c* (P or S). This is in contrast to the master event method in which time residuals are only taken for a single event, namely the master event.
4. For each event *k*, obtain a weighted mean of e_{ij} for all other events, where weights are based on the inter-event distance *i* to *k*. Following Andersen and Spottiswoode (2001), the weighted mean is taken in the sense of a weighted median to reduce the possible effect of outliers.
5. Relocate each event
6. End if $w_{rel} = 1.0$, else increase w_{rel} and go to step 3.

2.4.3 Testing of hybrid absolute-relative location method using synthetic data

Sample results are presented here for a synthetic data set consisting of:

1. Eight geophones at the corners of a cube 1000m on edge.
2. Velocity field (P and S) increasing linearly by 5% from X=0 to X=1000.
3. 10 events. The first is at X=300m, Y=200m and Z=0m (randomly chosen). The other nine events are spread along the Y and Z coordinates using a Gaussian random distribution with characteristic distance D=10m.
4. Each event is recorded at 80% of the sites, chosen randomly. S-waves were picked at 80% of the sites that recorded the events. A random error between 0ms and 1ms was added to each arrival. The number of arrivals varied between 7 and 14 out of a

maximum of 16. The travel time from sources to receivers was calculated based on the velocity at the midpoint of an assumed straight ray path. The rays therefore travelled 2½% faster to the four geophones at X=1000m and arrived anomalously earlier compared to rays to the four geophones at X=0m.

5. The events were located using the velocities at X=0.

Results are shown in the following diagrams. Figure 2.4.1 shows locations at three stages: true locations, absolute locations ($w_{rel} = 0.0$) and relative locations ($w_{rel} = 1.0$). It can be seen that the absolute locations moved about 20m along the +X directions and show a scatter of about 20m in X. The scatter is caused partially by the error in picking arrivals and partly by the variation in the geophones that were used for the locations. When the relative method is applied, the events group well along X≈320m and retain their relative positions along Y, but offset by about +4m. The convergence to a solution is shown in Figure 2.4.2. It can be seen that much of the scatter in the absolute locations is removed as solutions are done using relative differences.

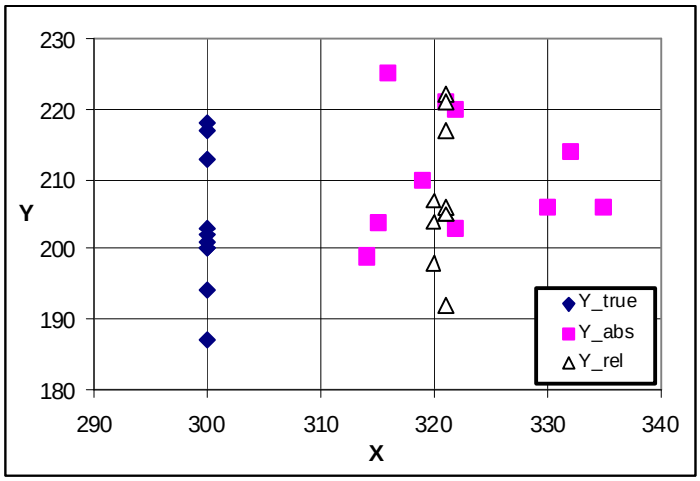

Figure 2.4.1: Locations of the 10 "random" events. Each event is represented by three symbols: "Y_true" is the true location; "Y_abs" is the location of each event separately and "Y-rel" is the location when 100% weight is given to the relative locations (w_{rel} = 1.0).

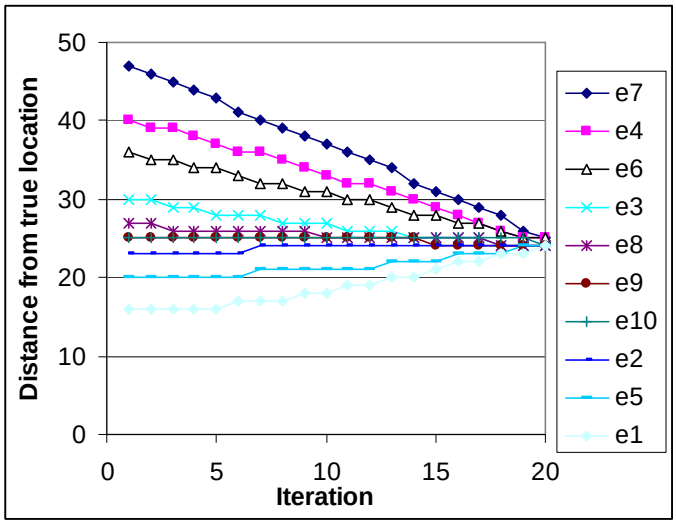

Figure 2.4.2: Migration of locations from absolute locations at iteration number 1 to fully relative locations at iteration number 20.

The locations were then repeated with two of the events fixed at their original locations, as shown with large symbols in Figure 2.4.3. The absolute (independent) locations of eight of the events are the same as shown in Figure 2.4.1. Arrival-time differences for the fixed events are given ten times the weighting of normal events. The relative locations are well behaved, returning to close to their true locations, as also shown in Figure 2.4.3.

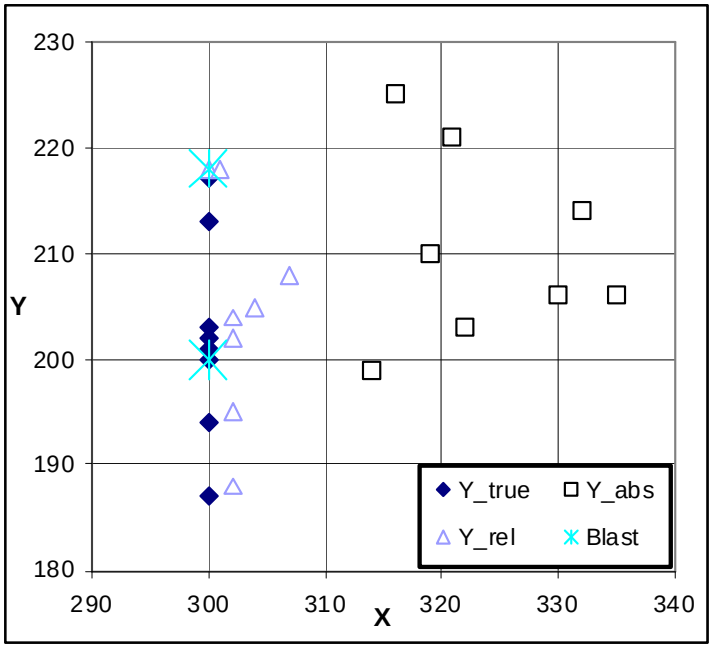

Figure 2.4.3: As for Figure 2.4.1, but with two events with fixed location, marked as "Blast".

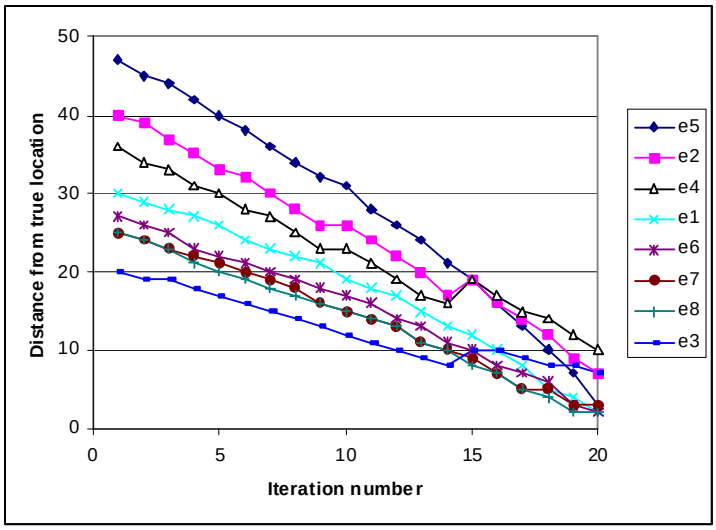

Figure 2.4.4: As for Figure 2.4.2, but with two events with fixed location.

2.4.4 Conclusion and discussion

The tests show that the program MLOC has worked well for synthetic data sets that show the same type of errors as are encountered with mine data. The relative method without a master event reduces the scatter in locations. When events with known locations are included, the events re-locate close to their true locations.

3 Include waveform similarity software in current seismic location algorithms

Miningtek's AURA software stores a small number of parameters (about 20) for the seismogram written by each geophone for a large number of events. The object is to compare these numbers for each geophone between all possible pairs of events. Well-correlated data will be used to provide values of the "double-differences" described by Waldhauser & Ellsworth (2000), as discussed above.

If the source mechanisms of two earthquakes are virtually identical, and they are located very close to one another, the signals recorded at a common recording station will be highly similar. The similarity of the waveforms can be identified using a number of methods, a few of which will be briefly mentioned.

3.1 Brief overview of waveform similarity identification methods

Waveform cross-correlations to identify similar waveforms can be performed in the time-domain (e.g. Deichmann & Garcia-Fernandez, 1992) or in the frequency domain (e.g. Poupinet et al., 1984). In the time-domain, the cross-correlations involve matching the waveforms 'wiggle for wiggle' whereas in the frequency domain, the modulus of the coherency spectrum is used (e.g. Got et al., 1994). A problem with the cross-correlation methods is that they are computationally and memory intensive for large data sets. Additionally, cycle skipping is a serious issue for monochromatic signals.

The relative amplitudes of the S/P ratio can also be used as a fairly crude measure of waveform similarity (e.g.: Young, *et al*., 2001). This method is less computationally and memory intensive than full waveform cross-correlations. Unfortunately, the relationship between S/P ratio and focal mechanism is non-unique.

In this project, the waveform similarity is being studied using a two-phase approach. The first phase involves the identification of similarities between events using the shape of cumulative energy and broad view of time differences. This method will be described in some detail in the next section. The second phase will examine the details of the similar events (identified using the cumulative energy comparisons) using waveform cross-correlation.

3.2 Cumulative energy comparisons

This method is used to get around problems associated with the classic method of waveform cross-correlation. Like the S/P ratio method, it is less computationally and memory intensive than full waveform cross-correlations, allowing large data sets to be processed.

The methodology is as follows.

1. Low-pass filter the signal (passing only the frequencies below the corner frequency (Figure 3.2.1a and b). The reason for filtering is that the energy is dominated by the frequencies above the corner frequency (82% of the energy in a seismogram is radiated at frequencies above the corner frequency). These high frequencies are caused by propagation of the source itself and are therefore unduly prone to "noise" caused by differences in source details.
2. Calculate the energy-cumulated trace from the filtered trace (Figure 3.2.1b and c). The time differences between the cumulative energy (for each event pair, recorded at a particular site and geophone orientation) at a number of preselected intervals are then calculated. In Figure 3.2.2, the cumulative energy intervals of 20%, 40%, 60% and 80% are used. The time differences $\delta t_1, \delta t_2, \delta t_3, \ldots, \delta t_n$ are computed for all event pairs where n

is the total number of time differences (Figure 3.2.2). The time differences are calculated between each possible pair of events in the data set, for every site and geophone orientation. The more similar the waveforms, the more similar the cumulative energy traces will be, resulting in similar time differences. The total number of time differences is:

$$n = 3 \cdot n_s \cdot n_i \qquad 3.2.1$$

where

n_s is the number of geophone sites

n_i is the number of intervals.

3. Sort the time differences and calculated the 'spread' using:

$$Spread = t_2 - t_1 \qquad 3.2.2$$

where

t_1 is the time difference at the 25th percentile

t_2 is the time difference at the 75th percentile

The calculation of the spread parameter is illustrated for one event pair in Figure 3.2.3. Similar events will have small time differences and correspondingly small spreads. Figure 3.2.4 shows a plot of the spread versus difference in hypocentral distance between event pairs and illustrates that those event pairs having a small spread (and therefore high similarity) are located closely in space.

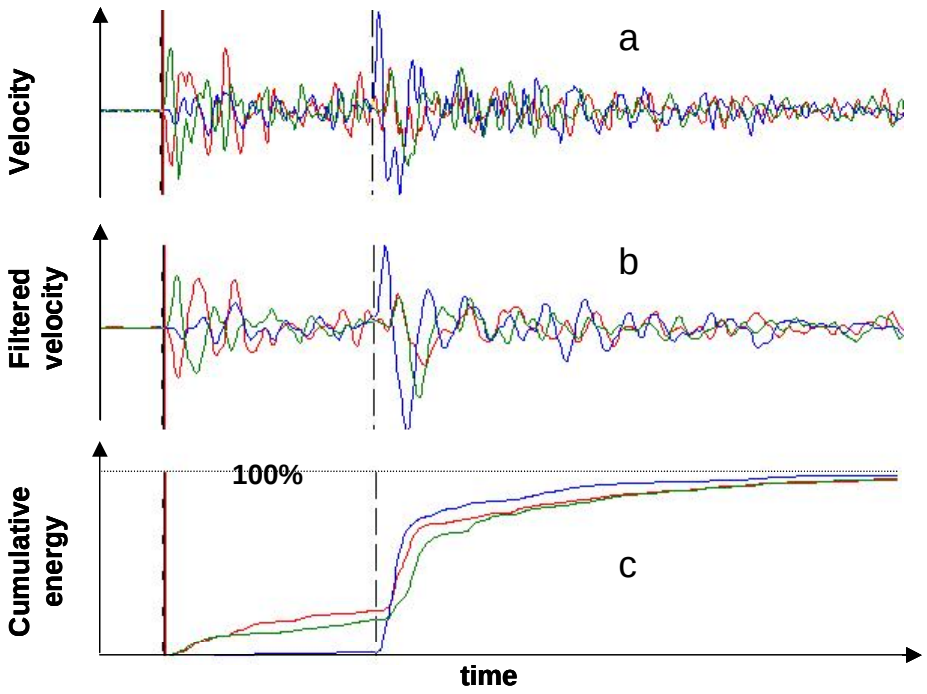

Figure 3.2.1: (a) Unfiltered velocity trace; (b) Low-pass filtered velocity trace; (c) Cumulative energy trace computed from the filtered velocity trace, normalised to the same total value.

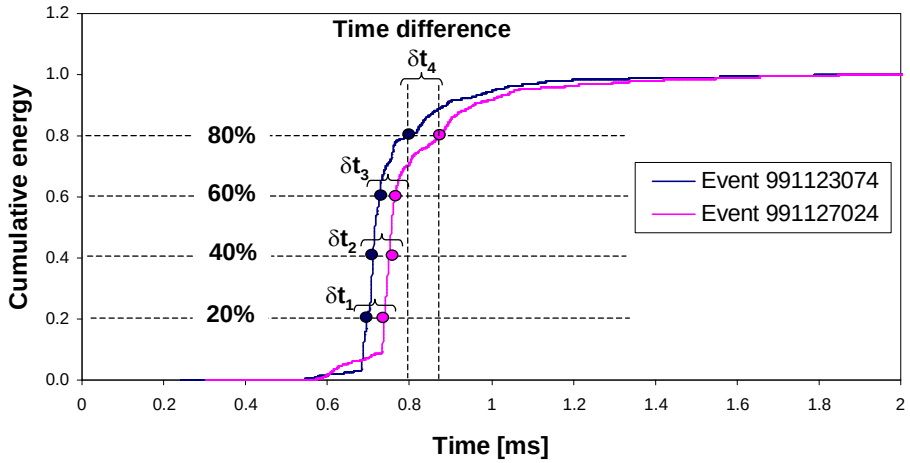

Figure 3.2.2: Calculation of time differences $\delta t_1, \delta t_2, \delta t_3, \delta t_4$ between the cumulative energy traces of an event pair (recorded at geophone site 1, geophone orientation 2).

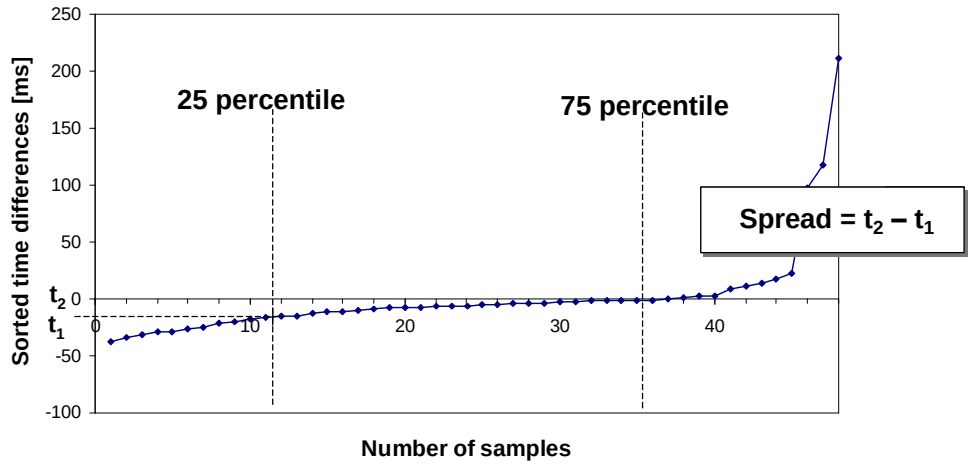

Figure 3.2.3: Sorted time differences $\delta t_1, \delta t_2, \delta t_3, \ldots, \delta t_n$ calculated for an event pair

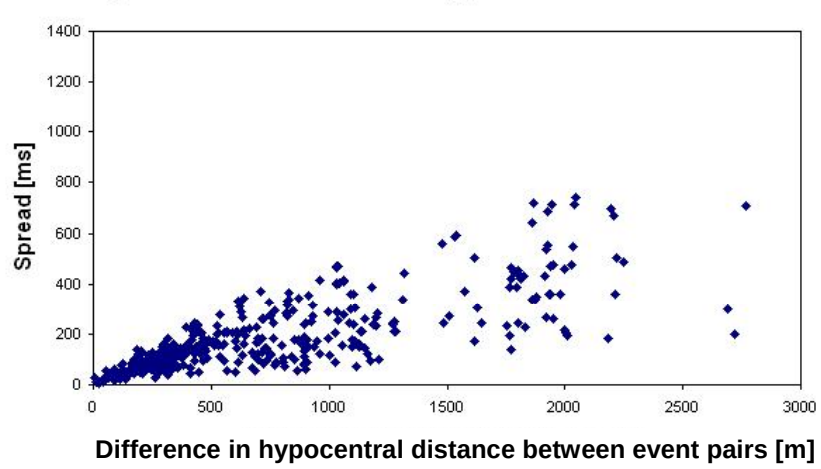

Figure 3.2.4 Correlation of spread and difference in hypocentral distance between event pairs.

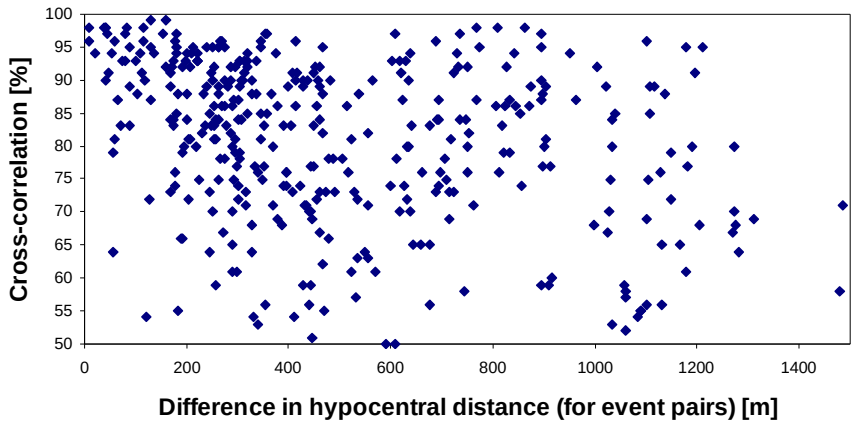

Figure 3.2.5 Cross-correlation of radiated energy flux at all geophones for all event pairs in a data set.

4 Improved seismic locations

The paper *Improved seismic event locations* was presented at the ISRM 2003–Technology Roadmap for Rock Mechanics Symposium in Johannesburg in September 2003 by Spottiswoode, S.M. and Linzer, L.M. It is attached in its unabridged form at the end of this report.

In the October 2003 report, we applied the hybrid location program, MLOC, to five data sets (TauTona shaft pillar, ARM 1# Pillar 56-29, ARM 2# 72NE54A, Bambanani and ARM 2# pillar 5342BP2). The results were shown in two ways: as plots of the pairs of events joined by vectors, and as plots of the distribution of the inter-event distances.

4.1 Early application of hybrid location program to data (September 2003)

The hybrid location program (MLOC) developed during this project was applied to five data sets (Table 4.1.1). The data sets were created using XTRIGQRY, a program that is part of the ISS suite of software, and contain information such as the event location, P and S-wave arrival times, P and S-wave velocities, geophone site co-ordinates etc. for each channel (i.e. per seismogram).

Table 4.1.1: Dataset parameters

Data set	Time period	No. Events relocated
TauTona	29/05/2001 – 15/02/2002	10 000
ARM 1# Pillar 56-29	01/01/2003 – 31/05/2003	3290
ARM 2# 72NE54A	03/01/2003 – 28/06/2003	1300
Bambanani	10/03/2003 – 28/07/2003	10 000
ARM 2# pillar 5342BP2	20/01/2003 – 30/06/2003	10 000

The original locations (i.e. the event locations given in the XTRIGQRY files) are compared with those computed using the absolute and hybrid methods in two ways: firstly, by visual comparison of event locations where the pairs of events have been joined by vectors, and secondly, by estimating the fractal dimension using inter-event distances between all event pairs.

In Figure 4.1.1, lines are drawn between pairs of events that have location errors < 25m (>95% of events); have occurred within 1 hour and 50m of one another; and have cross-correlation (r^2)>0.9 of PPV values. This method is only applied to the TauTona data set since we did not have the mine outlines for the other data sets at this stage in the project.

It is clear from Figure 4.1.1 that the hybrid locations are more tightly clustered than the original locations – this is especially clear for the events originating from the development ends below and within the shaft pillar.

In Figure 4.1.2 to Figure 4.1.5, the original locations (i.e. the event locations given in the XTRIGQRY files) are compared with those computed using the absolute and hybrid methods by estimating the fractal dimension D using inter-event distances between all event pairs. The fractal dimension describes the way the events are distributed in space, and can vary from 1 to 3: $D = 3$ indicates that the events are located in a 3-D distribution (e.g. like a cloud); $D = 2$ indicates that the events are organised along fracture planes; and $D = 1$ indicates that the events locate on lines.

After doing the analysis on the TauTona data (Figure 4.1.1), followed by the areas being considered under SIM 02-03-03 (Figure 4.1.2 to Figure 4.1.5), we noticed that the pattern of improved locations using the hybrid method persisted with the exception of ARM 2# 72NE54A (Figure 4.1.3). In three out of four cases, the close events became even closer (Figure 4.1.2, Figure 4.1.4 and Figure 4.1.5). In Figure 4.1.3, the absolute location method outperformed the hybrid and original locations for close events.

These trends will be examined more closely in SIM 02-03-03.

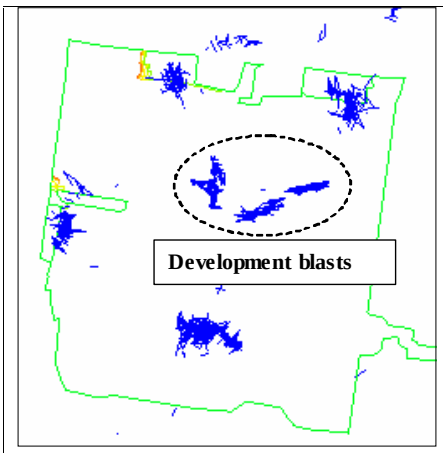

Hybrid Locations

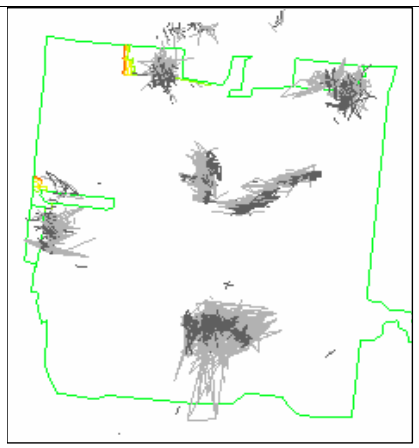

Absolute and Hybrid Locations

Figure 4.1.1 Seismicity in the TauTona Mine Carbon Leader Reef Shaft Pillar showing that the hybrid locations are much more tightly clustered than the absolute locations.

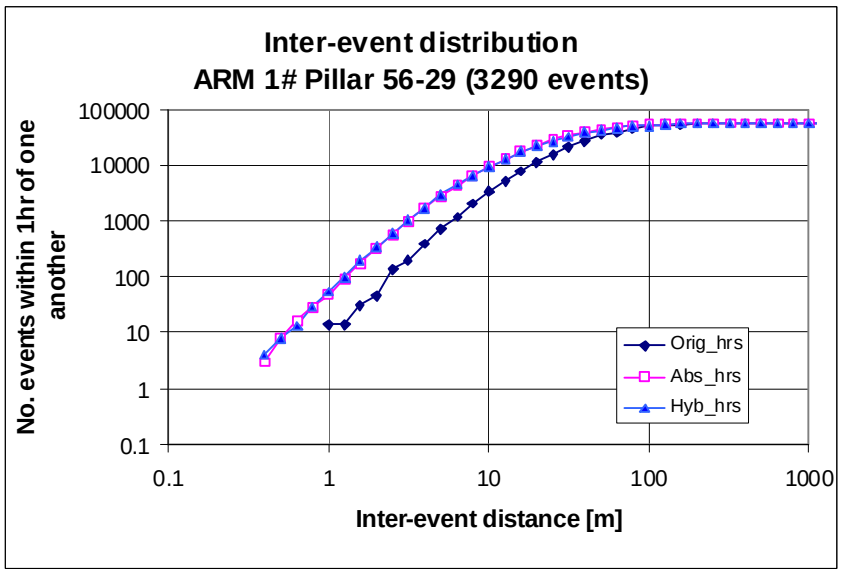

Figure 4.1.2: Distributions of inter-event distances between events occurring within 1hr of one another.

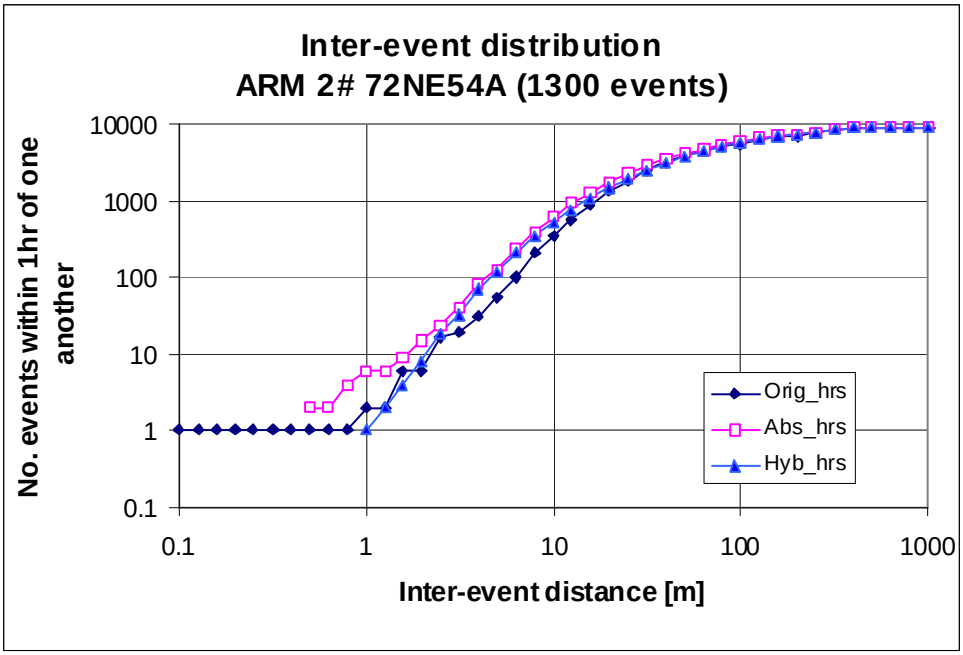

Figure 4.1.3: Distributions of inter-event distances between events occurring within 1hr of one another. The resolution of the locations is given to one metre. This caused the horizontal line for the original locations.

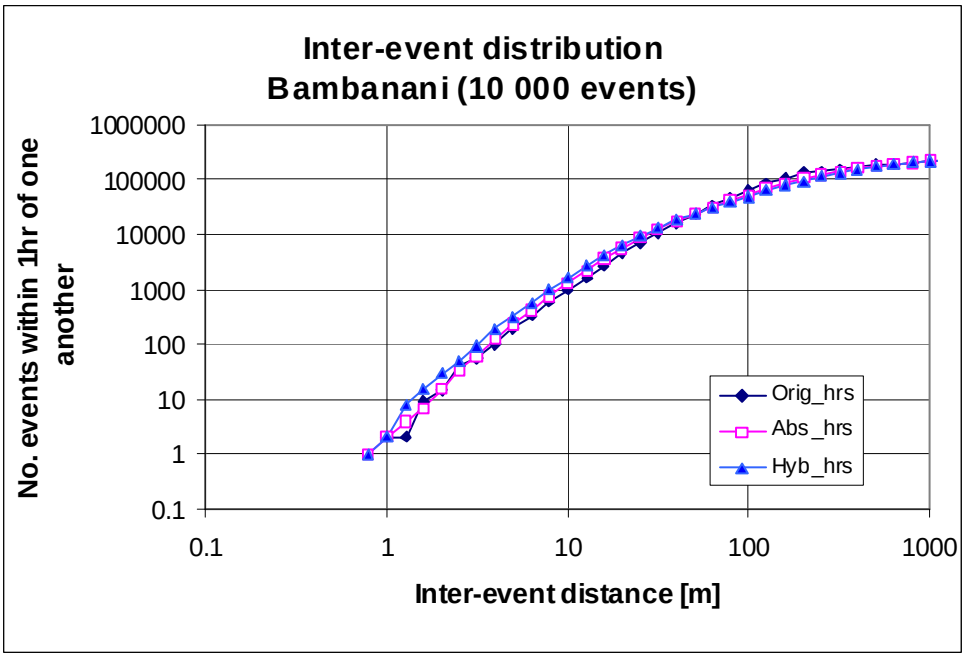

Figure 4.1.4: Distributions of inter-event distances between events occurring within 1hr of one another.

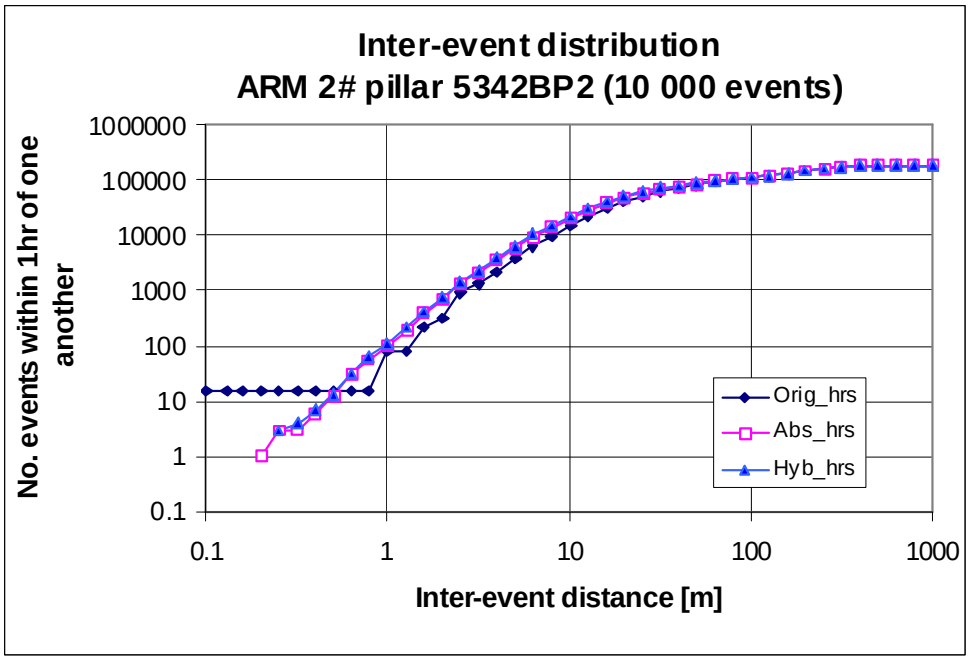

Figure 4.1.5: Distributions of inter-event distances between events occurring within 1hr of one another. The resolution of the locations is given to one metre. This caused the horizontal line for the original locations.

4.2 Detailed analysis of relocated events (TauTona).

In this report, the TauTona data set is analysed more closely. The data set was recorded from 29/05/2001 to 15/02/2002 and 10 000 of these events were relocated using MLOC. We are interested in the orientations of the vectors joining pairs of events that occurred within an hour of one another because it is likely that such events are mechanistically related and possibly show either the orientation of fracture planes, or the migration of events in a shear zone.

Five data sets in the TauTona shaft pillar were investigated and are labelled A to E in Figure 4.2.1. The sources of seismicity of the various areas are summarised in Table 4.2.1.

Table 4.2.1: Sources of Seismicity

Area	Source of seismicity
A	Complex mine layout
B	Development blasting
C	Breast-mining adjacent to North pillar abutment.
D	Breast-mining adjacent to North pillar abutment & closely approaching East pillar abutment
E	Development blasting

Area C was chosen for closer study because the mining is relatively simple geometrically. Area E was chosen for comparative purposes.

In Area C (Figure 4.2.1), the seismicity is a result of stoping, whereas the events in Area E are related to development. The difference between the on-reef and off-reef mining methods is evident from the temporal distribution of the events for areas C and E. In Figure 4.2.2, the

stoping events of Area C are spread over most of the 24 hr period whereas those of Figure 4.2.3 are grouped into approximately 4hrs.

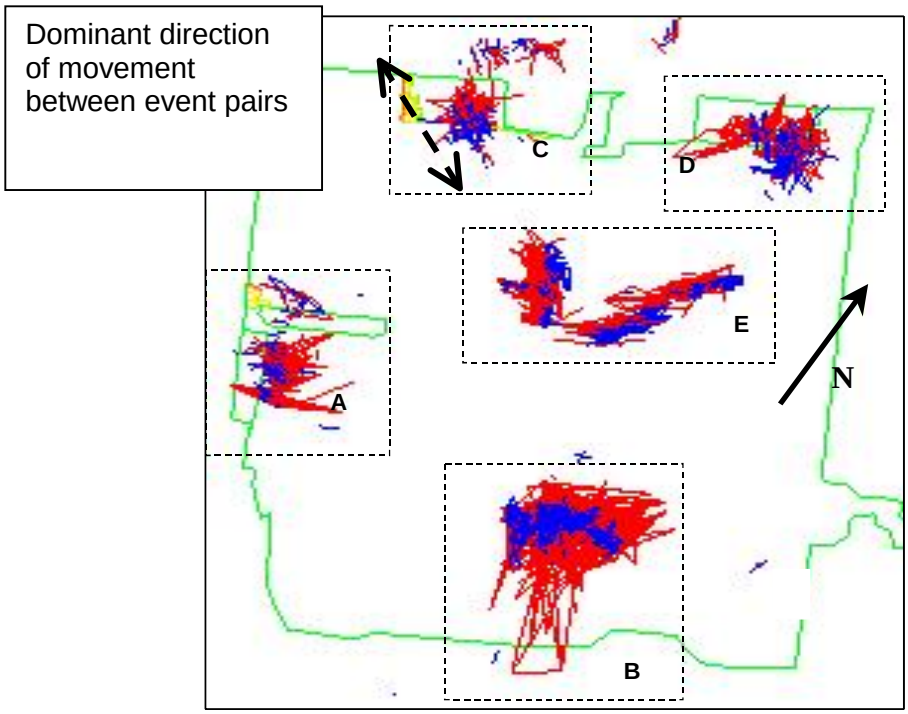

Figure 4.2.1: TauTona. Comparison of original and hybrid locations. Original locations are shown in red (light grey), hybrid locations are shown in blue (dark grey).

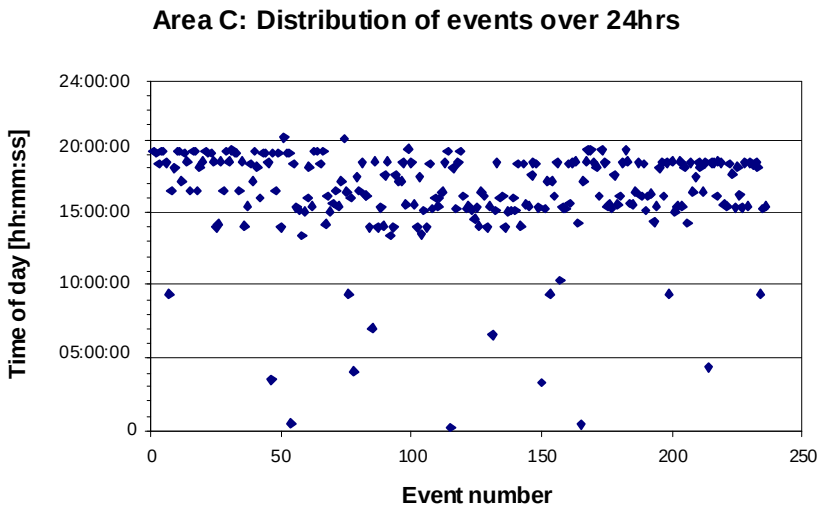

Figure 4.2.2: TauTona Area C. Distribution of events over 24 hr period.

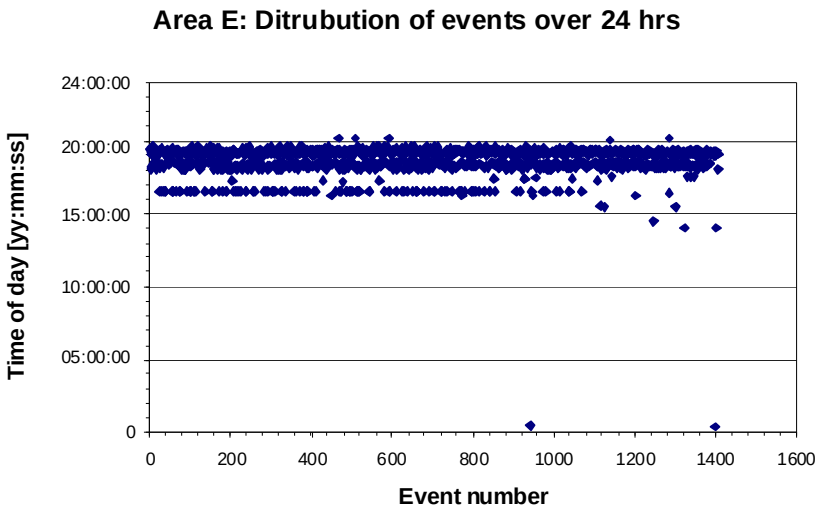

Figure 4.2.3: TauTona Area E. Distribution of events over 24 hr period.

In Figure 4.2.4 and Figure 4.2.5, the original locations (i.e. the event locations given in the XTRIGQRY files) are compared with those computed using the absolute and hybrid methods. The slope of each portion of the graph represents the fractal dimension D of the event pairs. The fractal dimension describes the way the events are distributed in space, and can vary from 1 to 3: $D=3$ indicates that the events are located in a 3-D distribution; $D=2$ indicates that the events are organised along fracture planes; and $D=1$ indicates that the events locate in lines. The 3-D distributions of events result from the event sources themselves being distributed over a volume. The location error and other sources of random error will cause further distribution over the volume.

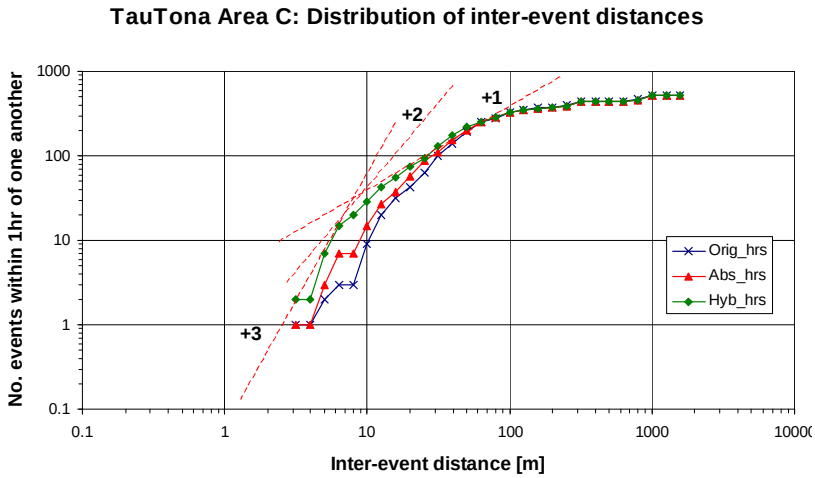

Figure 4.2.4: TauTona Area C. Distributions of inter-event distances between events occurring within 1hr of one another.

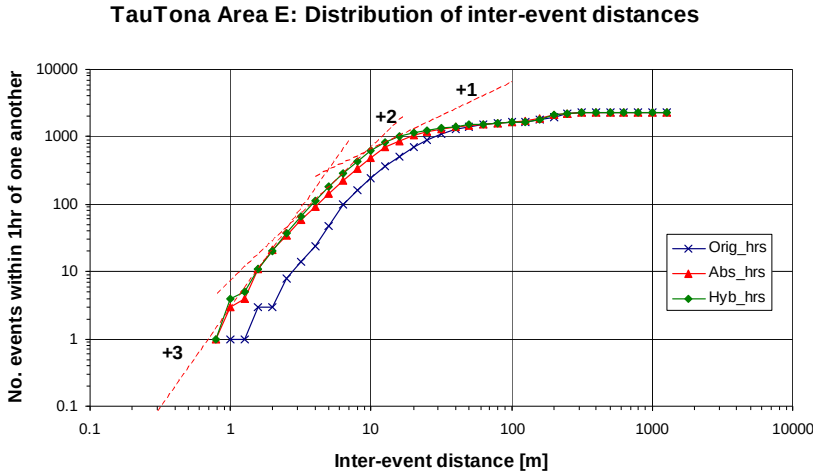

Figure 4.2.5: TauTona Area E. Distributions of inter-event distances between blast events occurring within 1hr of one another.

In the on-reef data set (area C), the close events become even closer after the hybrid location procedure, and the hybrid location method outperforms the absolute and original locations (Figure 4.2.4). In contrast, the hybrid and absolute locations for the off-reef data set (area E) are very similar and outperform the original location method (Figure 4.2.5).

The interpretations based on Figure 4.2.4 for Area C are as follows. From the intercept of the lines having slopes of 0 and +1, it is evident that the maximum distance between the pairs of events that occur within 1hr of one another is 100m. This will be the maximum length of the longwall.

The intercept of lines having slope of +1 and +2 is 13m. This is the maximum vertical dimension of the shear zone since the length of the zone would be the same as the length of the longwall. The intercept of lines having a slope of +2 and +3 is 7m. This indicates that the maximum location error is 7m (note that this is a combination of the location error and width of fracturing).

Figure 4.2.5 indicates that the location error for Area E is between 3m and 7m.

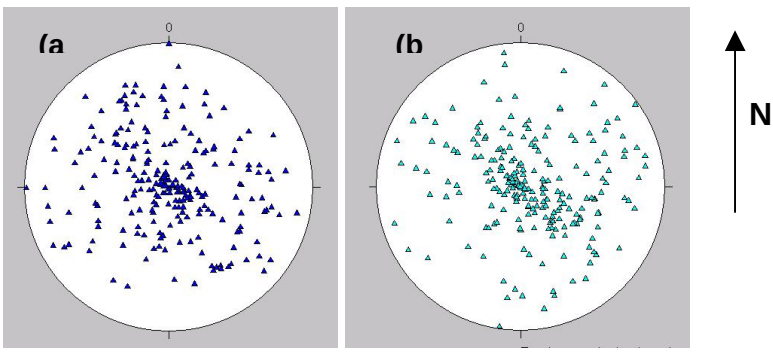

Figure 4.2.6 TauTona Area C. Stereographic projections showing orientations of the vectors connecting pairs of events occurring within 1hr or one another (a) Original catalogue locations (b) Hybrid locations.

Stereographic projections and rose diagrams are then used to plot the orientations of the vectors joining pairs of events that occurred within an hour of one another for Area C (Figure

4.2.6). The event pairs plotted for the absolute and hybrid locations show a similar grouping with moderate clustering of the vectors vertically (compare Figure 4.2.6a and b). The rose diagram plotted using the same data (Figure 4.2.7) shows that there is a relatively strong SE-NW trend to the vectors, which becomes slightly more emphasised in the hybrid location data. A possible explanation for vertical orientation of some of the vectors is that the hybrid location procedure moves the events along the direction of maximum location error (i.e. normal to reef). The SE trend of the vectors is a result of the events following the orientation of the faces being mined.

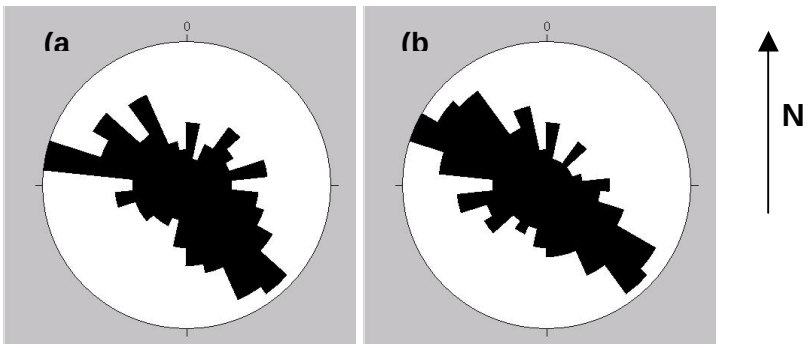

Figure 4.2.7: TauTona Area C. Rose diagrams plotted from vectors in Figure 4.2.6 (a) Original catalogue locations (b) Hybrid locations.

4.3 Summary of Methodologies

As this project draws to a close, it is appropriate to start developing a coherent description of the various methodologies that have been developed to improve locations in a manner that shows their respective roles. This report follows a talk entitled "Improved Seismic Event Locations" that was presented to the SA Geophysical Association on 30th January 2004. We hope to repeat this talk at the ISSI seminar in March 2004. Here we flesh the PowerPoint presentation out into text and diagrams.

4.3.1 Introduction

Mines can use improved seismic locations in a number of ways, such as

1. To provide Rapid, Reasonably accurate & robust locations for immediate response to communicate to mine staff and, for the largest events, to guide a rescue team.
2. Identification of active geological features, especially near the face or near intersections between features.
3. Quantification of seismicity. At present polygons are often drawn with difficulty to properly separate events from different areas.
4. Quantitative comparison with mining (e.g. Spottiswoode, 2004)
5. Effect of mining layouts. Good locations will be needed for research into lead-lags, for example, for SIM-040303.

Locations are generally achieved by minimisation of an error function. Generally the time residuals (differences between the observed and calculated arrival times of the seismic wave) for a single event are minimised using various least-squares procedures (Geiger, ~1900), as described by both ISSI and Miningtek in previous quarterly reports.

4.3.2 Selection of P- and S-wave arrivals & phase velocities

Locations are normally based on manually selected P- and S-wave arrival times. Figure 4.3.1 shows such picks (3 P-wave and 3 S-wave picks) on seismograms at three sites.

An algorithm has been developed as part of Miningtek's AURA software that selects P- and S-wave arrival times automatically.

Figure 4.3.2 shows that this algorithm successfully picked most of the arrival times for the seismograms shown in Figure 4.3.1 (3 P-wave and 2 S-wave picks). The picking was based on the energy envelope, where the energy was based on both kinetic and potential energy.

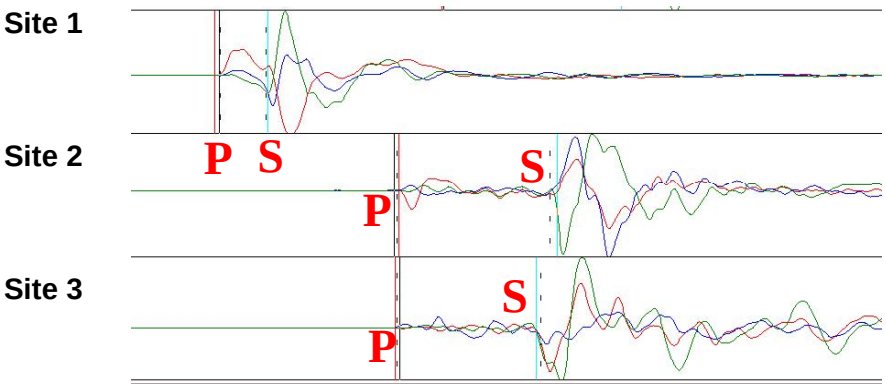

Figure 4.3.1: Seismograms from a mining-induced event recorded at three sites.

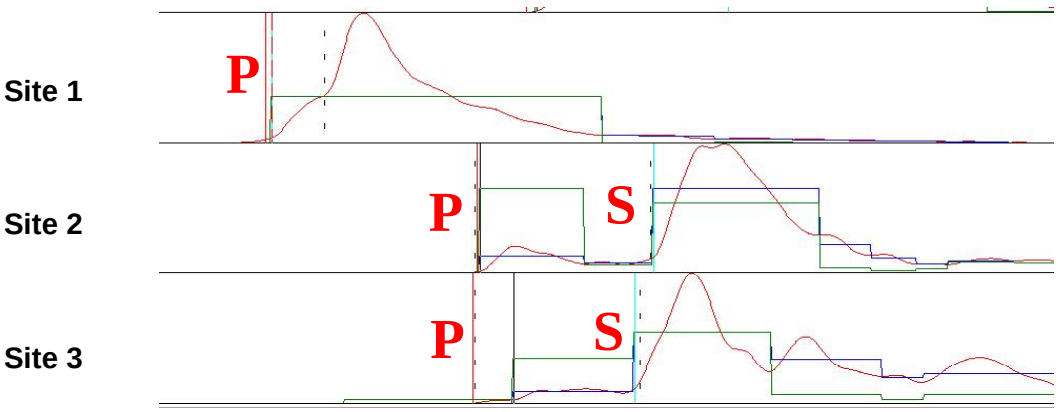

Figure 4.3.2: Envelope function (red), construction lines (green and blue) and automatically selected arrival-time picks.

Construction lines are also shown to illustrate the process of following the amplitudes and changes in amplitudes between successive minima or near minima of the energy function. A P-wave arrival is picked when there is a rapid change in the energy level. If the energy decays sufficiently and then rises again sharply, an S-wave arrival is picked.

This algorithm works quite well but as with all automated arrival-time picking algorithms, it is prone to errors when seismograms are less than ideal. There are three types of non-ideal seismograms:

1. **Poor signal-to-noise ratio**. The skilled human eye is still a better filter of noise than any automatic procedure for seismograms with low signal-to-noise ratios. This is especially true when the noise is not very well described (i.e. is more random).

2. **Emergent arrivals**. Often small amplitude signals precede the main energy pulse. A common mistake in locating such events is to pick the P-wave arrival at the very first low-energy pulse and then the S-wave arrival at the high-energy pulse. We are then trying to locate a different event with P waves compared to the event located with S waves. This naturally increases the location error.

3. **Multiple events** within the same triggered time window. This occurs commonly during and following the blast sequence. This problem is likely to get worse as mines adopt centralised blasting using electronic delays because post-blast seismicity will then more often occur simultaneously across the entire mine.

4.3.3 Development of velocity models

Wave velocities are controlled by many factors, such as rock type, stress (gravity, tectonics & mining induced) and mining-induced fracturing. Velocities generally increase with increasing stress until significant fracturing occurs. Stress fields are controlled by depth of burial, previous and current tectonic activity and finally mining induced stresses.

Typical phase velocities in the Wits gold mines are about V_P = 6 km/s and V_S = 3.7 km/s. Mine-wide networks generally locate events based on constant velocity values and keep using these values. These are assumed to be accurate to a few percent. Figure 4.3.3 shows a travel-time plot that may be used to estimate velocities based on known event locations and arrival times. The velocities were calculated from the inverse of the slope of the two lines.

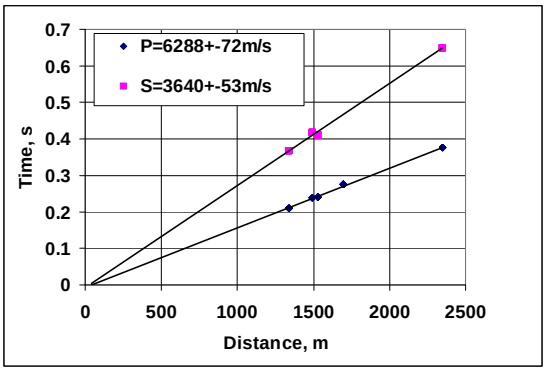

Figure 4.3.3: Travel-time plot used to estimate P- and S-wave velocities.

4.3.4 Poor network configurations

It is well known that geophone sites in mine networks are often constrained by access tunnels to be close to the typically planar ore body. All the geophones might be within 100m of a plane that is several kilometres in extent. This results in two possible problems:

1. Poor location accuracy in the direction normal to the plane of the geophones. The location accuracy over much of the network in the direction perpendicular to reef might be more than the true spread of locations. This problem is addressed in AURA by applying “Loose restriction to reef” which creates a bias that pulls events towards the reef. If a small weighting factor is applied, this bias is very effective for poor geophone configuration, for example for events well outside the network. Locations in well-constrained regions are unaffected by this bias.
2. The location settles in to a local minimum that is not the global minimum. Our solution to this problem is to image the location across planes formed by sets of three nearby geophones and then to re-solve the location. In most cases, the location returns to the same solution. In these cases, this precaution was not necessary. In the few cases

where two or more minima have been found, the software selects the location with the lowest RMS error.

4.4 Absolute and relative locations

Previous quarterly reports and the paper by Spottiswoode and Linzer (2003) have referred to the use of relative locations. In Spottiswoode and Linzer (2003) we introduced a hybrid absolute-relative location methodology. Here we show further results of this method applied to a large data set from a mine. The smallest located events out of 37 000 relocated events are shown in Figure 4.4.1. The hybrid locations appear to be sharper than the mine's catalogue data. Two types of sharpening are visible:

1. Development blasts follow better-defined lines, as shown by arrows.
2. The hybrid locations show clearly defined grouping, such as the two regions within ellipses. These events locate in the final pillar positions between the raises. It should be noted that the most recent face outlines were earlier than the most recent seismicity so as not to crowd the diagram with face outlines.

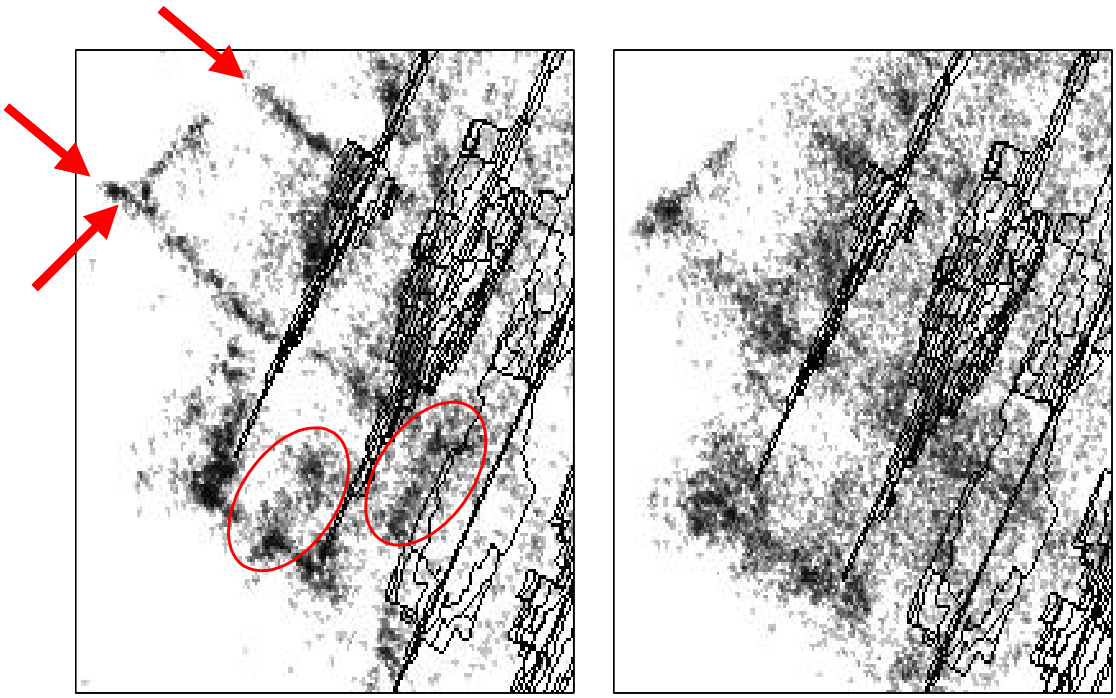

Figure 4.4.1: Locations performed by standard processing on a mine are shown as "catalogue locations" (right). These same events have been relocated using the hybrid method using the same P- and S-wave arrival times (left).

4.5 Use of waveform similarity in automatic locations

This section is based on the report of December 2003, but with many changes due to improved analysis.

4.5.1 Cumulative energy comparisons

This method is used to get around problems associated with the classic method of waveform cross-correlation. Like the S/P ratio method, it is less computationally and memory intensive than full waveform cross-correlations, allowing large data sets to be processed using normal PC RAM. The methodology has been described in detail in Section 3.2. Applying the methodology,

we can calculate times at which percentile values of energy arrive (Figure 4.5.1) and spread parameters (Figure 4.5.2). Similar events will have similar time differences and correspondingly small time spreads, as indicated in Figure 4.5.2. Figure 4.5.3 shows a plot of the time spread versus inter-event distance between event pairs, and demonstrates that those pairs with small time spreads (and therefore high similarity) are located closely in space.

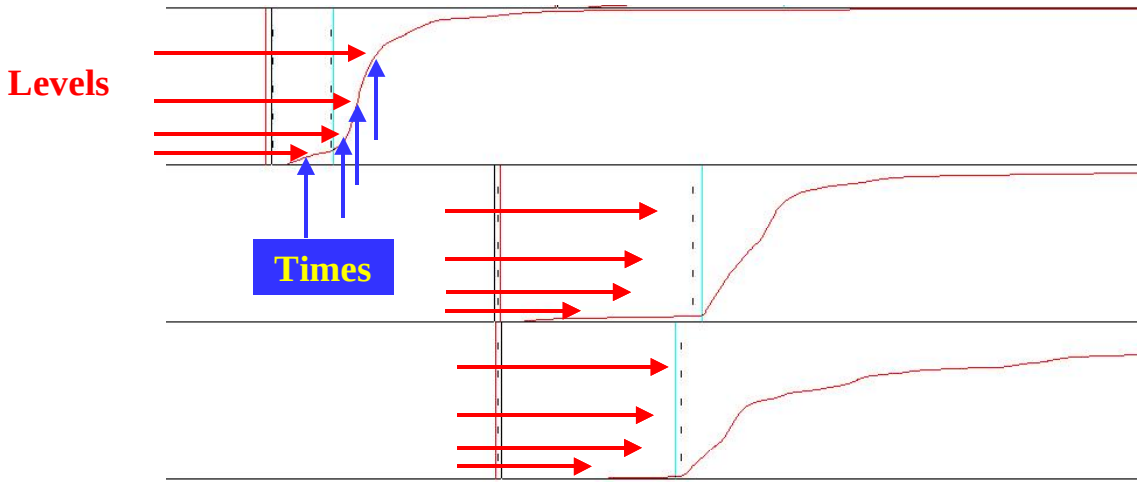

Figure 4.5.1: Times at which cumulative energy thresholds are exceeded for one geophone (top) and two sample cumulative energy plots.

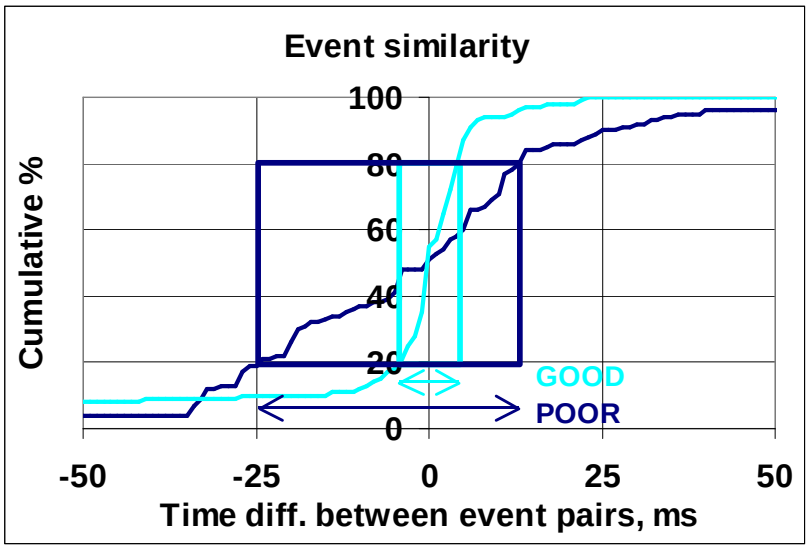

Figure 4.5.2: Sorted time differences $\delta t_1, \delta t_2, \delta t_3, \ldots, \delta t_n$ calculated for two event pairs. The light coloured distribution is an event pair with better correlation than the event pair plotted as the dark-coloured distribution.

In Figure 4.5.3 we compare inter event distances of all pairs between 85 events from a mine with the time spread as defined above. It can be seen that all the data lie above a bounding line with apparent velocity of 10m/ms. The practical interpretation is that each event (A) is within $D=t_{AB}*10$m/ms distance of any other event (B), where t_{AB} is the time spread of energies between events A and B.

For example, using Figure 4.5.3, if an event B is found with a time spread t_{AB}=10ms when paired with event A, then event B occurred within 100m of event A, as shown by the horizontal and vertical arrows. We then have a robust location for event A, namely the location of event B. We also have an estimate of the error (D) in this estimate, namely D=100 m.

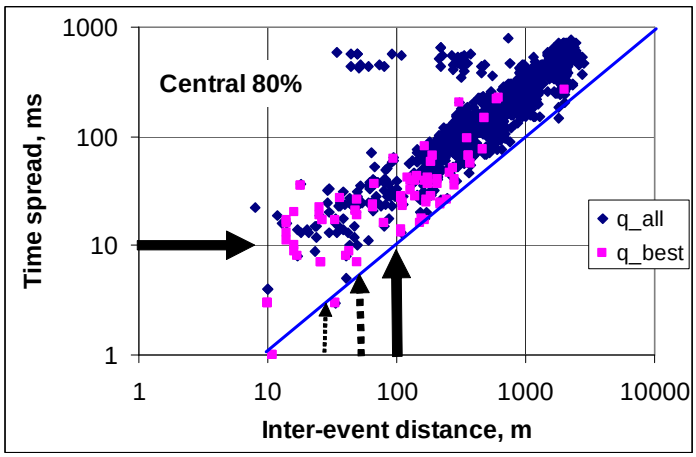

Figure 4.5.3: Correlation of spread and difference in hypocentral distance between event pairs. The smallest spread values for each event are labelled "q_best".

5 Error of seismic parameters

Richardson & Jordan (2002) reprocessed the seismograms of 228 events recorded at Mponeng, Elandsrand and TauTona to confirm the catalogued source parameters stored on the mines' seismic systems. These researchers used the method outlined in Andrews (1986) and calculated displacement, velocity and acceleration spectra for every waveform of each event. Each event's spectra were median stacked and integrated (for frequencies less than the Nyquist frequency) and the energy E, moment M_o, static stress drop $\Delta\sigma$ and source radii r were calculated. The comparison between the recalculated values and mine catalogue values are shown in Figure 4.5.1.

Richardson & Jordan (2002) found that the recalculated moments correlated well (correlation coefficient of 0.94) with the catalogued moments, although the catalogued values tended to be larger than the recalculated values (Figure 4.5.1a). They found that the amount of scatter due to uncertainty was greater than the mean difference between the recalculated values and catalogued values. Both measures of M_o had an estimated error of approximately 2%.

The recalculated corner frequency f_o matched the catalogue well for $f_o < 200$Hz (Figure 4.5.1b). The mean difference between the two measures was found to be approximately 6Hz which was less than the expected uncertainty, whereas for $f_o > 200$Hz, the mean difference was about 20Hz. Due to the 300Hz ceiling (a restriction imposed by the mine's seismic processing software), the catalogue consistently underestimated the f_o of small events.

In Figure 4.5.1c, the events that had energy E < 500J in the catalogue were underestimated because these events correspond to those whose f_o were underestimated. However, for those events that had E > 500J, the recalculated values matched the catalogued values well within the expected uncertainty (10% for the Richardson & Jordan study, and 12% for the mine catalogues).

The value of the source radius r determined by Richardson & Jordan correlated well with the catalogued values (correlation coefficient of 0.85) for $r \geq 10$m (Figure 4.5.1d). Once again the scatter due to uncertainty was greater than the mean difference between the two measures. For $r \leq 10$m, the catalogue consistently overestimated r because of the 300Hz cut-off.

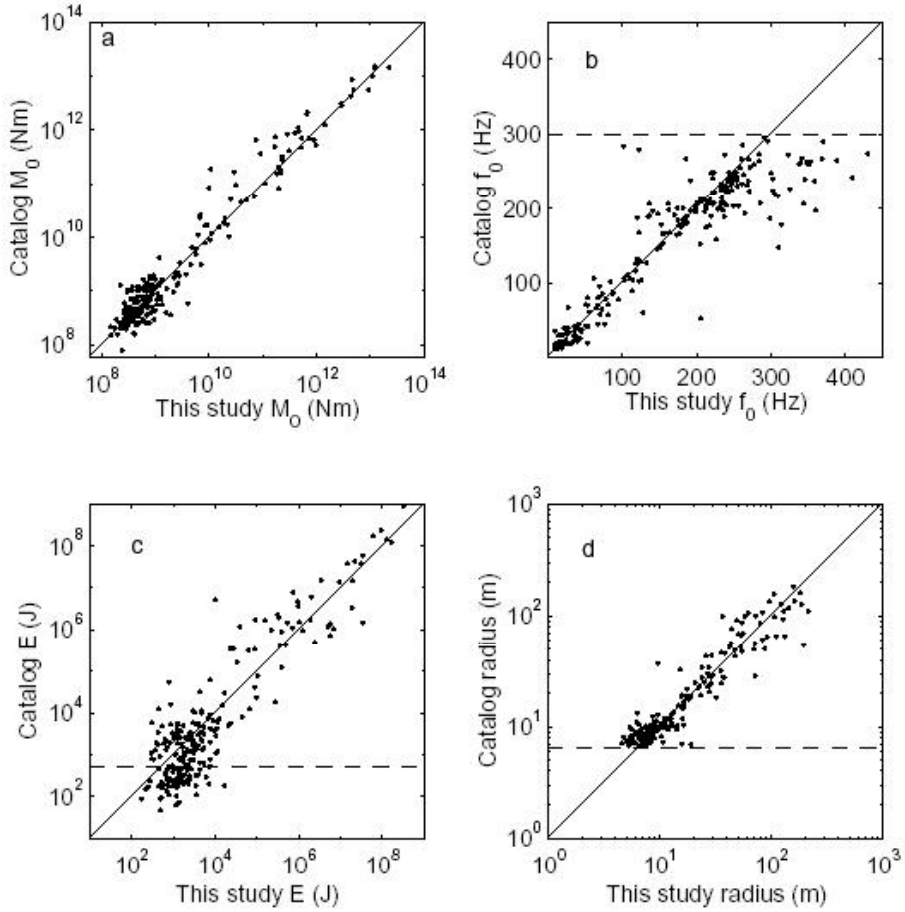

Figure 4.5.1 Comparison between values calculated in the Richardson & Jordan study and the mine catalogue values of seismic moment M_o (a), corner frequency f_o (c), energy E (c), and source radius r (d) for 228 events recorded at Mponeng, Elandsrand and TauTona. Solid line = slope of 1. Dashed line in (b) and (d) represent the 300Hz f_o ceiling for the catalogue data. Values below the dashed line in (c) are underestimated in the catalogue data due to the 300Hz f_o ceiling (from Richardson & Jordan, 2002).

6 References

Andrews DJ (1986): Objective determination of source parameters and similarity of earthquakes of different size. In: *Earthquake Source Mechanics* (S Das, J Boatwright, and CH Scholz eds.). Am. Geophys. Union, Washington, D.C., **6**, pp.259-267.

Fehler M, Phillips WS, Jones R, House L, Aster R. and Rowe C (2000): A method for improving relative earthquake locations. *Bull. Seism. Soc. Am.* **90**, pp. 775 – 780.

Finnie GJ, Spottiswoode SM, and Amidzic D (2002): Observations of Bimodal Seismicity In Deep Gold Mines. *Abstract at ISSI seminar*, March 2002.

Got J-L, Fréchet J, and Klein FW (1994): Deep fault plane geometry inferred from multiplet relative relocation beneath the south flank of Kilauea. *J. Geophys. Res.* **99 No. B8**, pp.15375-15386.

Got J-L, Okubo P, Machenbaum R, and Tanigawa W (2002): A Real-Time Procedure for Progressive Multiplet Relative Relocation at the Hawaiian Volcano Observatory, *Bull. Seism. Soc. Am*, **92**, pp.2019 – 2026

Jones, R and Stewart RC (1997): A method for determining significant structures in a cloud of earthquakes. *J. Geophys. Res*. **102**, pp.8245 – 8254.

Milev AM, Spottiswoode SM, Rorke AJ, and Finnie GJ (2001). Seismic monitoring of a simulated rockburst on a wall of an underground tunnel, *J. S. A. Inst. Min. Metall*., **101**, pp.253-260.

Nadeau R, Foxall W, and McEvilly T (1995): Clustering and periodic recurrence of Microearthquakes on the San Andreas fault at Parkfield, California, *Science*, **267**, pp.503-507.

Richardson E and Jordan TH (2002): Seismicity in Deep Gold Mines of South Africa: Implications for Tectonic Earthquakes. *Bull. Seismol. Soc. Am*. **92** pp.1766-1782.

Rowe C, Aster R, Jones R, Borchers B, and Fehler M (2002): Using automated high-precision repicking to improve delineation of microseismic structures at the Soultz geothermal reservoir. *Pure. Appl. Geophys*. **159**, pp.563-596.

Rubin AM (2002): Using Repeating Earthquakes to Correct High-Precision Earthquake Catalogs for Time-Dependent Station Delays. *Bull. Seismol. Soc. Am*. **92**, pp.1647-1659.

Rubin AM, Gillard D, and Got J-L (1999): Streaks of microearthquakes along creeping faults. *Nature*, **400**, pp.635-641.

Sambridge MS and Kennett BLN (2001): Seismic event location: Nonlinear inversion using a neighbourhood algorithm. *Pure Appl. Geophys*. **158**, pp.241-257.

Spottiswoode SM (1993): Seismic attenuation in deep-level mines. *3rd Intl Symposium on Rockbursts and Seismicity in mines*, Balkema, pp.409-414.

Spottiswoode SM and Milev A (1998): The use of waveform similarity to define planes of mining-induced seismic events, *Tectonophysics* **289**, pp.51-60.

Spottiswoode SM (2004): A seismic and modelling analysis of dip-pillar mining. Submitted to: *2nd International Seminar on Deep and High Stress Mining*, South African Institute of Mining and Metallurgy.

Waldhauser F, Ellsworth WL and Cole A (1999): Slip parallel seismic lineations on the northern Hayward Fault, California, *Geophys. Res. Lett*. **26**, pp.3525-3528.

Waldhauser F, and Ellsworth WL (2000): A double-difference earthquake location algorithm: method and application to the northern Hayward fault, California. *Bull. Seism. Soc. Am*. **90**, pp.1353-1368.